Self-reduced Co-TiO_2 photocatalysts for peroxymonosulfate activation: efficient ciprofloxacin degradation and dynamic charge transfer

Shuzhe Zhang[1a], He Wang[1a], Gang Chen[b], He Zheng[c], Yanhua Song[a], and Haifeng Zou[*a]

[a] Department of Chemical Engineering and Applied Chemistry, College of Chemistry, Jilin University, Qianjin Street 2699, Changchun 130012, China.

[b] State Key Laboratory of Supramolecular Structure and Materials, College of Chemistry, Jilin University, Changchun 130012, China.

[c] State Key Laboratory of Inorganic Synthesis and Preparative Chemistry College of Chemistry Jilin University, Changchun 130012, China.

Corresponding Author:

[*]E-mail: haifengzou0431@sohu.com

[1] These authors contributed equally to this work.

Materials

All chemicals were not further purified. Isopropyl titanate (TTIP), $Co(NO_3)_2 \cdot 2H_2O$, $KSHO_5$ and Na_2CO_3 were purchased from Macklin Biochemical Co., Ltd. Cetyltrimethylammonium bromide (CTAB) and hydrofluoric acid (HF) was supplied by national pharmaceutical reagents Co., Ltd. Ethylene glycol (EG) was obtained from Tianjin Tiantai Chemical Co., Ltd.

Characterizations

The structural and morphological features of the synthesized catalysts were systematically characterized using advanced analytical techniques. Field-emission scanning electron microscopy (FE-SEM, Hitachi S4800) and high-resolution transmission electron microscopy (HR-TEM, Tecnai F20) were employed to visualize the surface topography and structural details. The crystalline phases were identified by

powder X-ray diffraction (XRD, DX-2700) measurements conducted at room temperature. Surface chemical composition and electronic states were analyzed using X-ray photoelectron spectroscopy (XPS, VG ESCALAB 250), while electron spin resonance spectroscopy (ESR, JEOL JES-FA 200) was utilized to investigate defect states.The porous texture and specific surface area were determined through nitrogen adsorption-desorption experiments performed on a Micromeritics ASAP 2020HD88 analyzer. Optical absorption characteristics were studied via UV-vis-NIR spectroscopy (PerkinElmer Lambda 950), and charge carrier recombination behavior was assessed using photoluminescence spectroscopy (Edinburgh Instruments FLS 1000). Additionally, photoelectrochemical properties were examined with a CH Instruments 660e electrochemical workstation configured in a standard three-electrode setup.

Photocatalytic Performance Evaluation

The photocatalytic reduction of CIP was investigated using an aqueous CIP solution (20 mg/L, 50 mL) containing 20 mg of catalyst. Prior to illumination, the suspension was magnetically stirred in darkness for 30 min to achieve adsorption-desorption equilibrium. Subsequently, 5 mg of PMS was added to the solution. During simulated solar irradiation, reaction aliquots (1 mL) were collected at regular time intervals and immediately centrifuged to separate catalyst particles. And then analyzed by UV-vis spectroscopy to track degradation kinetics (λ_{max} = 335 nm).

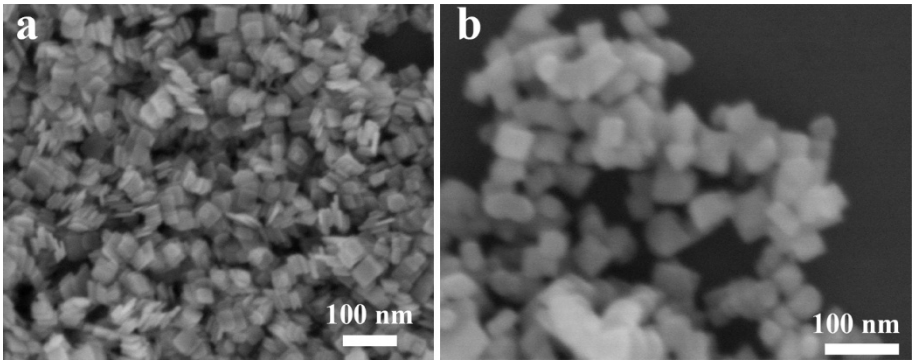

Fig. S1. SEM images of (a)TO and (b) CoBTO

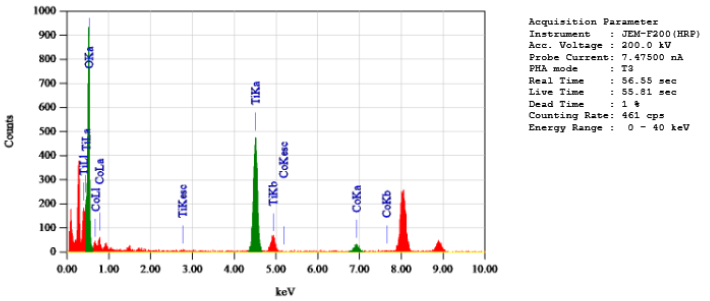

Thin Film Standardless Standardless Quantitative Analysis
Fitting Coefficient : 0.3661

Element	(keV)	Mass%	Counts	Sigma	Atom%	Compound	Mass%	Cation	K
O K	0.525	48.67	4880.51	1.28	74.25				1.1913
Ti K (Ref.)	4.508	46.94	5607.19	1.34	23.93				1.0000
Co K	6.924	4.39	395.23	0.48	1.82				1.3259
Total		100.00			100.00				

Fig. S2. TEM mapping diagram and atomic ratio of CoTO

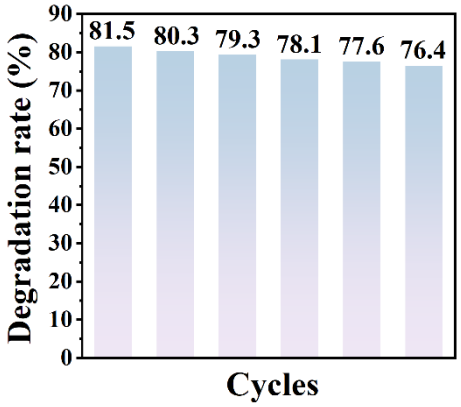

Fig. S3. Cyclic degradation efficiency of CoTO

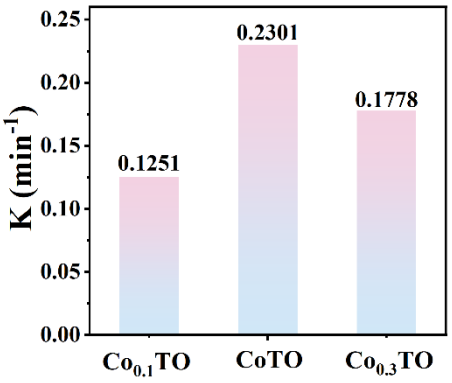

Fig. S4. Photocatalytic degradation efficiency of CIP over samples with different Co doping concentrations

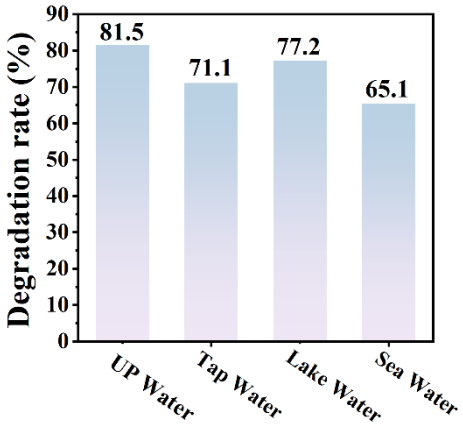

Fig. S5. CIP degradation efficiency by the Vis/CoTO/PMS system in various water matrices

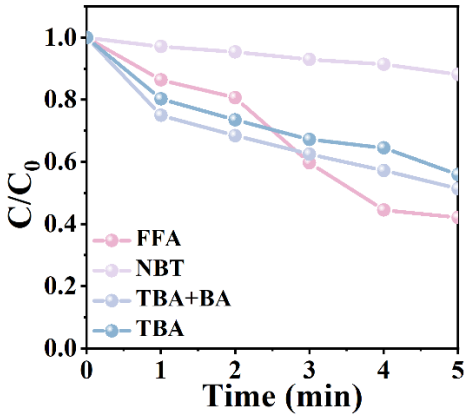

Fig. S6. Consumption kinetics of chemical probes in the Vis/CoTO/PMS system for CIP degradation

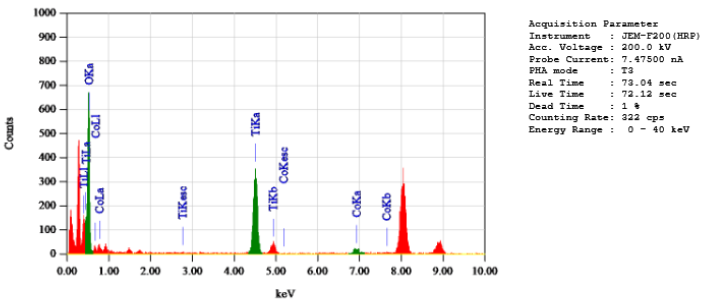

Thin Film Standardless Standardless Quantitative Analysis
Fitting Coefficient : 0.4808

Element	(keV)	Mass%	Counts	Sigma	Atom%	Compound	Mass%	Cation	K
O K	0.525	49.86	3651.58	1.51	75.14				1.1913
Ti K (Ref.)	4.508	45.96	4009.61	1.55	23.15				1.0000
Co K	6.924	4.17	274.56	0.55	1.71				1.3259
Total		100.00			100.00				

Fig. S7. TEM mapping diagram and atomic ratio of CoTO after the cycles

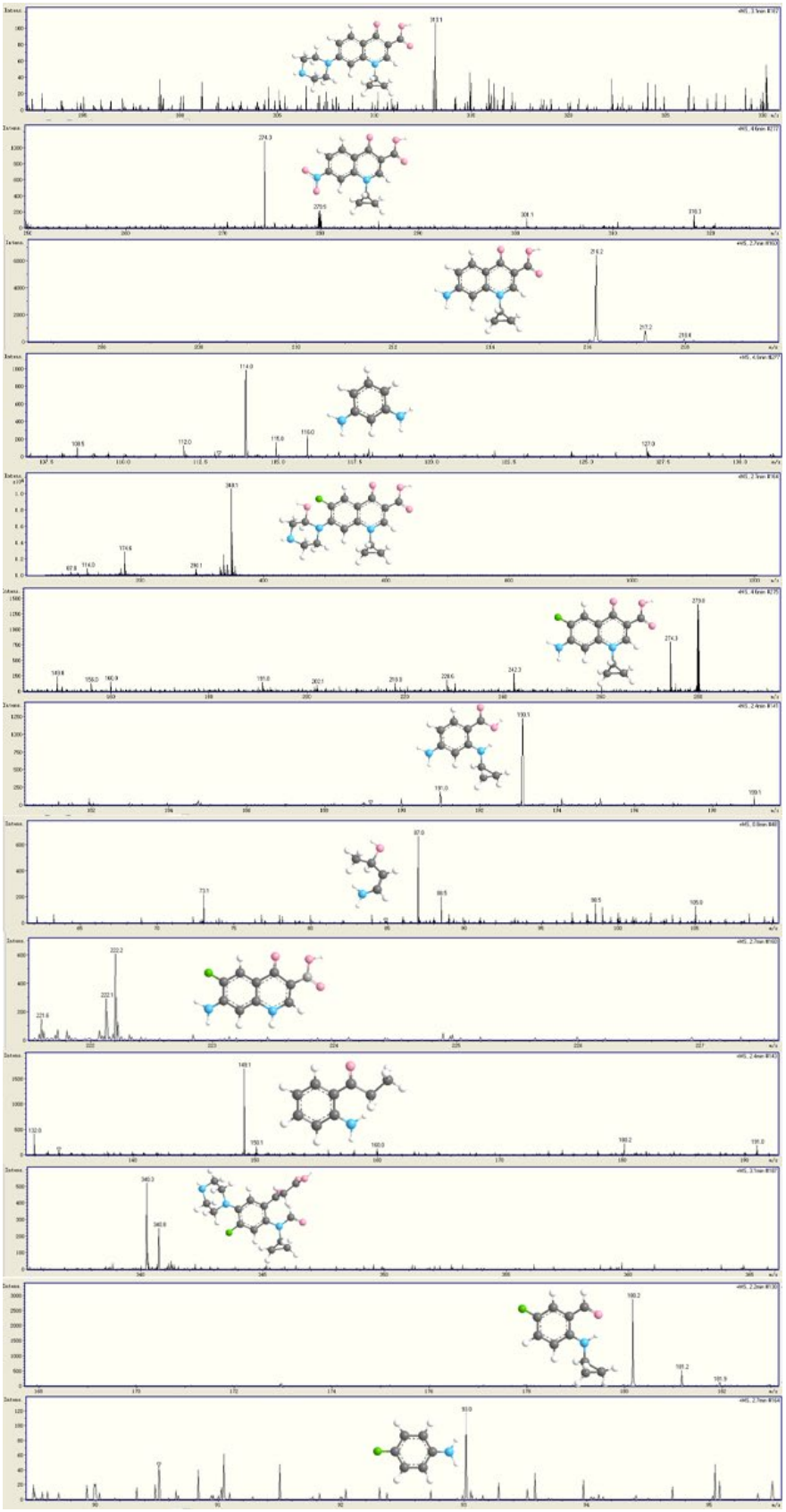

Fig. S8. LC-MS analysis of CIP during its degradation process

Table S1. Comparison of photodegradation performance of CIP by various photocatalysts

Catalyst	Catalyst Conc. (g/L)	Catalyst Conc. (g/L)	CIP Conc. (mg/L)	Degradation efficiency (%)	Time (min)	Ref.
CoTO	**0.4**	**0.1**	**20**	**81.5**	**5**	**This work**
β-CD-CoWO4350	0.2	0.13	20	80.9	60	[1]
$LFPBC_{0.5}$	1.0	0.51	10	89.8	90	[2]
S3	0.6	1.0	20	82.6	30	[3]
BOF-5	0.6	0.6	10	70.0	30	[4]
MnO_2/CuO-0.3	0.1	0.1	10	66.1	6	[5]
MX/Cu-G-CN	0.5	1.27	10	88.8	150	[6]

Table S2. Relative contribution of various reactive species to CIP photodegradation

Reactive species	Scavenger	Inhibition rate (%)	Relative contribution (%)
h^+	EDTA-2Na	52.5	24.2
SO_4•$^-$	EtOH	51.0	23.5
$^1O_2$	L-H	46.6	21.4
•O_2^-	CH_3Cl	39.7	18.3
e^-	$KBrO_3$	12.1	5.6
•OH	IPA	15.4	7.1

Table S3. The second-order reaction rate constants of probes, quenchers and deprotonated organics with ROS

	•OH ($M^{-1}\cdot s^{-1}$)	$SO_4^{\bullet-}$ ($M^{-1}\cdot s^{-1}$)	$^1O_2$ ($M^{-1}\cdot s^{-1}$)	$O_2^{\bullet-}$ ($M^{-1}\cdot s^{-1}$)
TBA	6.0×10^8	4.0×10^5	3.04×10^3	-
FFA	1.5×10^{10}	-	1.2×10^8	-
BA	5.9×10^9	1.2×10^9	-	-
NBT	1.9×10^9	-	-	5.9×10^4

Table S4. ICP-OES analysis of the solution after the cycles

	Co	Ti
CoTO	0.43%	0.0008%

References

1. G. Zhang, X. Fan, H. Chen, Z. Li, H. Lei, G. Chen, N. Fu and X. Ren, β-cyclodextrin-modified cobalt tungstate with abundant nanoconfined channels activating peroxymonosulfate for Ciprofloxacin degradation: Performance optimization and mechanism study, *Colloids and Surfaces A: Physicochemical and Engineering Aspects*, 2026, **740**, 140198.
2. Y. Fu, Y. Yi, W. Chen, Y. Wang, Z. Diao and J. Qi, Unveiling the critical roles of iron and phosphorus in magnetic biochar derived from lithium-extraction residues of retired $LiFePO_4$ batteries for peroxymonosulfate activation toward ciprofloxacin degradation, *Bioresource Technology*, 2026, **448**, 134324.
3. X. Yu, S. Wang, P. Mo, H. Gao and C. Wang, Charge transfer and PMS activation in high-entropy spinel oxide-based Z-scheme heterojunctions for ciprofloxacin degradation, *Journal of Science: Advanced Materials and Devices*, 2026, **11**, 101100.
4. Y. Zhao, C. Yuan, Y. Yu, X. Zhang, S. Tu, N. Tian and H. Huang, Elucidating charge transfer and radical mechanisms in PMS-activated dot-on-plate $Fe_2O_3/Bi_{12}O_{17}Cl_2$ heterojunctions for enhanced photocatalysis, *Journal of Colloid and Interface Science*, 2026, **708**, 139774.
5. Y. Tian, W. Sun and G. Zhang, Engineering Mn/Cu bimetallic redox couples and mesoporous architecture for peroxymonosulfate-mediated pollutant removal, *Colloids and Surfaces A: Physicochemical and Engineering Aspects*, 2026, **734**, 139430.
6. Y. Peng, H. Zhang, C. Zhang, Q. Li, C. Yang, Z. Peng, X. Hu, C. Huang, M. Li, J. Deng and C. Tang, Cu single-atom sites boosting peroxymonosulfate activation on MXene/Cu-g-C_3N_4 for $\bullet O_2^-$ and $^1O_2$ driven antibiotic removal, *Surfaces and Interfaces*, 2026, **80**, 108153.